ChemComm

Chemical Communications

ROYAL SOCIETY
OF CHEMISTRY

COMMUNICATION
Haixing Li *et al.*
Robust binding between secondary amines and Au
electrodes

60 YEARS
ANNIVERSARY

COMMUNICATION
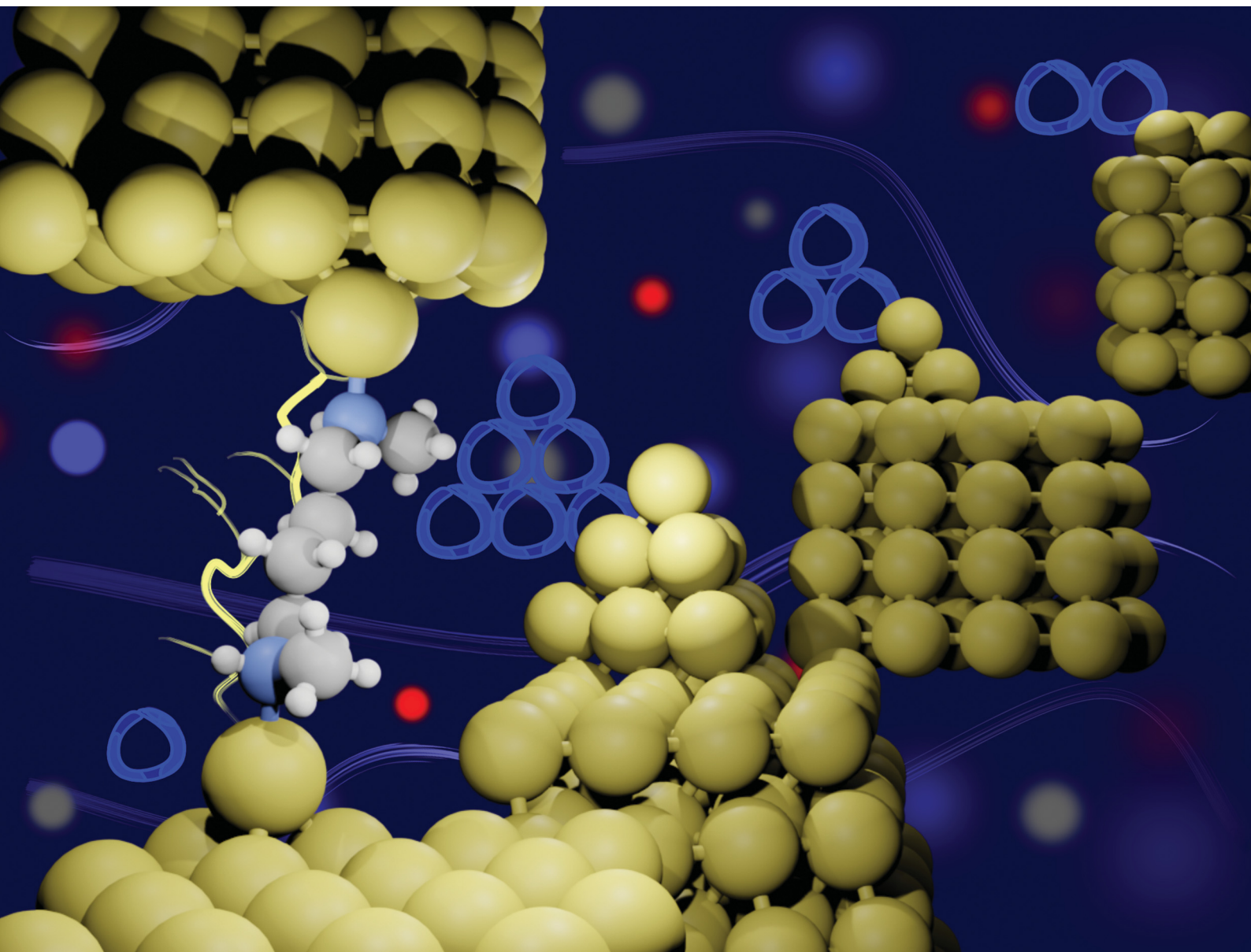
Robust binding between secondary amines and Au electrodes†

Weiyi Guo, [iD] [a] Timothy Quainoo,[b] Zhen-Fei Liu [iD] [b] and Haixing Li [iD] *[a]

While primary amines are one of the most widely used linker groups for forming single-molecule junctions, it remains elusive whether and how the substitution of one hydrogen in a primary amine with a methyl group (secondary amine) can alter its functional properties as a linker group. Here we show that a robust binding between a secondary amine and an Au electrode is absent with the use of a non-coated Au tip and is achieved when in contact with a wax-coated Au tip, which we propose is catalyzed by the more frequent formation of Au adatoms in measurements with a wax-coated tip.

A robust linkage between a molecule and a metal surface provides a basis for probing and tuning electronic characteristics of molecular-scale devices.[1] Among many, primary amines ($R–NH_2$) are a widely-used chemical group for linking molecular backbones to metal electrodes through dative interactions between the nitrogen lone pair and undercoordinated Au atoms ($N\rightarrow Au$).[2–4] In addition, a new type of N–Au electronically-transparent contact is formed between primary amines and Au atoms in an ionic environment constructed by a polar solvent propylene carbonate (PC) and supporting electrolyte tetrabutylammonium perchlorate ($TBAClO_4$) under a high tip bias voltage of 360 mV or above.[5] Linkers that carry an alkyl group such as methyl sulphide or dimethyl phosphine, similar to primary amines, can also form robust donor–acceptor interactions with Au.[6] In contrast, secondary amines ($R–NHCH_3$), due to the steric hindrance produced by the methyl group, are considered to have a weaker interaction with Au electrodes than primary amines and thus are rarely used as a linker group for forming molecular junctions.[4] We note that the electron-donating methyl group on the nitrogen can possibly enhance the donor–acceptor $N\rightarrow Au$ bond, but this effect is negligible

compared to its steric effect. In one example, secondary and tertiary amines were employed as terminal linker groups in saturated heterocyclic cyclohexane derivatives, 1,4-piperazine and 1,4-diazabicyclo[2.2.2]octane, where the steric hindrance effect of the methyl groups was weakened.[7]

In this study, we show that through the use of a wax-coated Au tip, secondary amines can form a robust contact with Au electrodes. We carry out single-molecule conductance measurements of N,N'-dimethylbutane-1,4-diamine (molecule **1**) and find a higher Au–molecule–Au junction formation probability for measurements with a wax-coated tip, in a polar solvent PC or under dry conditions, than with a non-coated tip in a nonpolar solvent 1,2,4-trichlorobenzene (TCB). Our experimental measurements combined with binding-energy calculations using density functional theory (DFT) reveal that the generation of undercoordinated Au surface adatoms in a wax-coated tip enhances the access of N lone pairs to Au atoms, and thus the $N\rightarrow Au$ binding between secondary amines and Au metal. Furthermore, the same single molecule conductance was observed for primary and secondary amine-terminated butane molecules, indicating that a similar electronic coupling with the Au metal was achieved for primary and secondary amine anchor groups. This result provides new insight about the interactions that secondary amines exhibit with metal surfaces, which may further expand their use in organic electronics.

Molecules **1** and **2** (structures are shown as the insets of Fig. 1b), comprising a butane backbone terminated with secondary or primary amine groups, respectively, are examined in this work. We first perform conductance measurements of 1 mM concentration of the target molecules in a nonpolar solvent TCB using the scanning tunneling microscope-break junction (STM-BJ) technique,[4,8] as illustrated in Fig. 1a. We repeatedly form and break single-molecule junctions thousands of times and construct one-dimensional (1D) conductance histograms as shown in Fig. 1b. We observe the same molecular conductance $\sim 10^{-3} G_0$ for both **1** and **2** under a −90 mV tip bias (a total of −100 mV bias is applied in the circuit with a 100 kΩ resistor in series). Importantly, we observe a more well-defined conductance peak

[a] Department of Physics, City University of Hong Kong, Kowloon 999077, Hong Kong SAR, China. E-mail: haixinli@cityu.edu.hk
[b] Department of Chemistry, Wayne State University, Detroit, Michigan 48202, USA
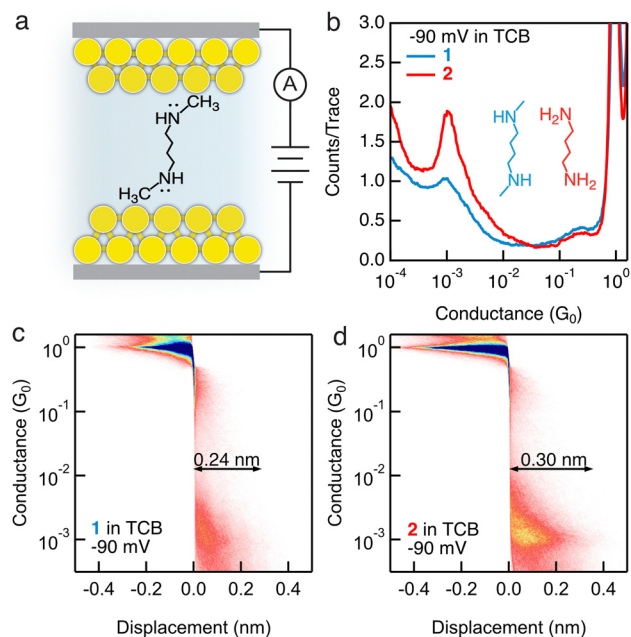
Fig. 1 (a) Schematic of the STM-BJ setup with a non-coated tip to measure the single-molecule conductance in a nonpolar solvent. (b) Logarithmically binned 1D histograms of **1** and **2** measured in TCB under a −90 mV tip bias. Inset: chemical structures of **1** (blue) and **2** (red). (c) and (d) 2D histograms of (c) **1** and (d) **2** created from the same data that were used to generate the 1D histograms in (b).

for **2** than for **1**; when we further carry out measurements under 90 mV, 910 mV, and −910 mV, we again observe a clearer conductance peak for **2** than for **1** under all measured biases, as shown in Fig. S1 (ESI†). We then compile all conductance–displacement traces into two-dimensional (2D) histograms to analyze the molecular junction elongation length. We observe a less distinct molecular plateau for **1** (Fig. 1c and Fig. S2a–c, ESI†) than for **2** (Fig. 1d and Fig. S2d–f, ESI†) under all biases, indicating that secondary amine terminal groups cannot access or form robust dative interactions with Au atoms in the same manner as primary amine terminal groups, likely due to the steric-blocking of the methyl group present in the secondary amines, which is consistent with previous reports.[4]

We next conduct STM-BJ measurements of a 1 mM solution of **1** in a polar solvent PC[9,10] with a wax-coated Au tip and a mechanically polished Au slug. We observe more intense conductance signatures for **1** measured in PC under −90, −320, 90, and 320 mV bias voltages (example traces, 1D, and 2D histograms are provided in Fig. 2b–e; Fig. S3 and S4, ESI†), than those displayed for measurements in TCB, indicating more robust junction formations of **1** in a polar solvent and with a wax-coated Au tip than in a nonpolar solvent and with a non-coated Au tip. When we compare the conductance features for **1** and **2** in PC (Fig. 2), we observe clear conductance peaks for both, in contrast to what we see in the measurements performed in TCB. The results so far suggest that the polar environment, the use of a wax-coated Au tip, or both enables a reliable binding of secondary amines to Au atoms, comparable to what is achieved by primary amines. We reproduce this result

using **1** purchased from a second manufacturer (Fig. S5 and Part IV, ESI†). We further test a hexane backbone terminated with secondary amines and observe a clear conductance feature for measurements with a wax-coated tip in PC, but not with a non-coated tip in TCB (Fig. S6 and S7, ESI†), in agreement with our results for the butane backbone. Next, we carry out measurements of **1** in polar solvent PC with an additional electrolyte (0.1 M TBAClO$_4$), in which the mobile ions in the solution can generate an electric double layer at the metal–solution interface. We do not observe clear molecular conductance signatures (Fig. S8, ESI†). We think that the formation of an electric double layer composed of specifically absorbed ions as well as solvated ions at the charged metal surface can potentially hinder the accessibility of N lone pairs to the Au atoms, preventing junction formation.

We observe that during the retraction of the STM tip in each break-junction measurement, both the Au point contact and the single molecule junction plateau lengths are significantly increased for measurements conducted with a wax-coated tip than those performed with a non-coated tip. Specifically, the plateau length of single Au–Au atomic contacts at one conductance quantum ($1G_0 = 2e^2/h$) is ∼0.8 nm when a wax-coated tip is used (Fig. S9a and b, ESI†), in contrast to the ∼0.18 nm plateau length when a non-coated tip is used (Fig. S9c and d, ESI†). We note that this observed difference in the plateau lengths of the Au–Au point contacts is associated with the use of a wax-coated or non-coated tip, but not with the presence or absence of a solvent (Fig. S9, ESI†). Similarly, we observe a molecular junction elongation length of ∼1.67 nm (Fig. 2e and f) for **1** and **2** measured in PC, substantially larger than the elongation length of ∼0.24 nm for **1** and ∼0.3 nm for **2** measured in TCB (Fig. 1c and d). This observation is consistent with a previous work in which an increased molecular junction elongation length was observed by the use of a flexible gold-coated quartz nanopipette tip in comparison to a regular solid gold tip.[11] We hypothesize that these increased plateau lengths of Au–Au point contacts and single molecule junctions result from either the increased likelihood of the junctions to form growing Au atomic chains and concurrent contact geometry rearrangements during the STM tip retraction,[12] or an usual slipping of the Au tip when it is coated with wax.

In order to distinguish the impact of a polar solvent and a wax-coated tip for promoting the –NHCH$_3$–Au binding, we further carry out measurements in the absence of a polar solvent. Here we introduce the target molecules through a 1 mM solution in isopropanol, dry the Au slug substrate in air, and perform the measurements with a wax-coated tip under dry conditions (Fig. 3a). We observe a clear conductance signature for **1** measured under dry conditions (Fig. 3b), similar to what we see in measurements of **1** with a wax-coated tip and polar solvent, but in contrast to what we observe in measurements of **1** with a non-coated tip. Therefore, the use of a wax-coated tip, rather than the polar solvent, plays a critical role in enabling the robust binding between the secondary amines and Au electrodes. Furthermore, we observe an increased plateau length of Au–Au point contact of ∼1.75 nm (Fig. S10a, ESI†), as well as an increased molecular plateau length of ∼2.75 nm (Fig. S10b, ESI†), in comparison to the ones measured with a non-coated tip. We hypothesize that this
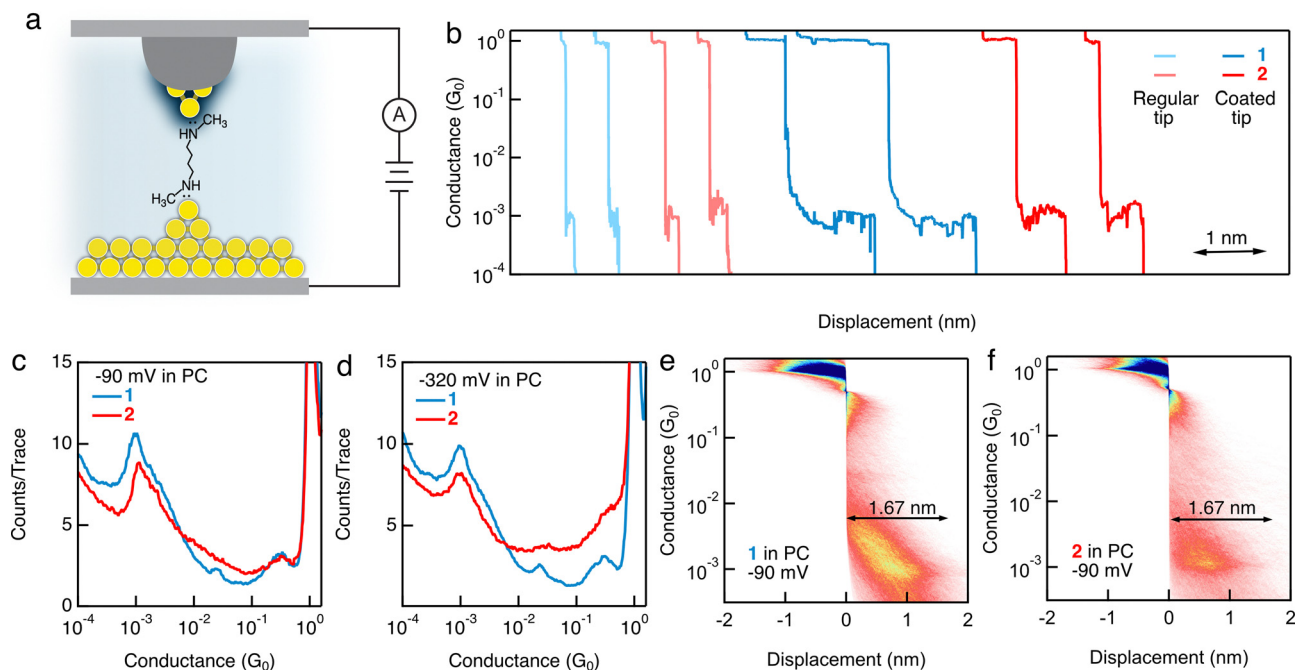
Fig. 2 (a) Schematic of an STM-BJ setup with a wax-coated tip for measuring molecular conductance in PC, a polar solvent. The dark blue shade near the tip represents an enhanced interfacial electric field. (b) Representative individual traces showing the ∼0.2 nm and ∼1.5 nm molecular plateau lengths observed for **1** and **2** measured with non-coated or coated tip. (c) and (d) 1D histograms of **1** and **2** measured in PC under a (c) −90 mV and (d) −320 mV tip bias. (e) and (f) 2D histograms of (e) **1** and (f) **2** measured under a −90 mV tip bias.
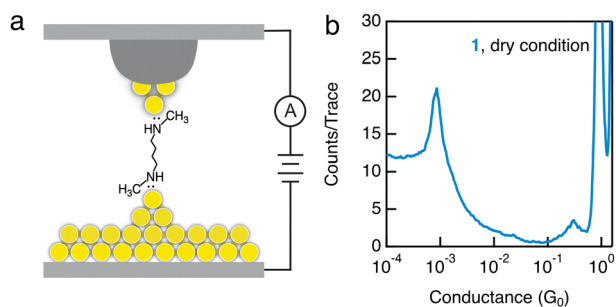
Fig. 3 (a) Schematic of the STM-BJ setup with a wax-coated tip for measuring molecular conductance under dry conditions. (b) 1D histogram of **1** measured under dry conditions with a 90 mV tip bias.

enhanced binding of secondary amines to Au electrodes is due to specific local Au surface structures generated only with the use of a wax-coated Au tip.

We next use DFT-based binding-energy calculations to illustrate that the types of local Au structures that enhance binding with secondary amines are in the form of Au adatoms. Fig. 4 shows the binding configurations between **1** and different Au local structures, computed using DFT (see ESI† for computational details), with the binding energies listed in Table 1. In general, the strongest binding with both types of amines is observed for Au adatoms, followed by Au trimers, and the binding of amines with the Au pyramids is the weakest (for the two types of pyramids, the binding with two-layer pyramids is stronger than with three-layer pyramids for both types of
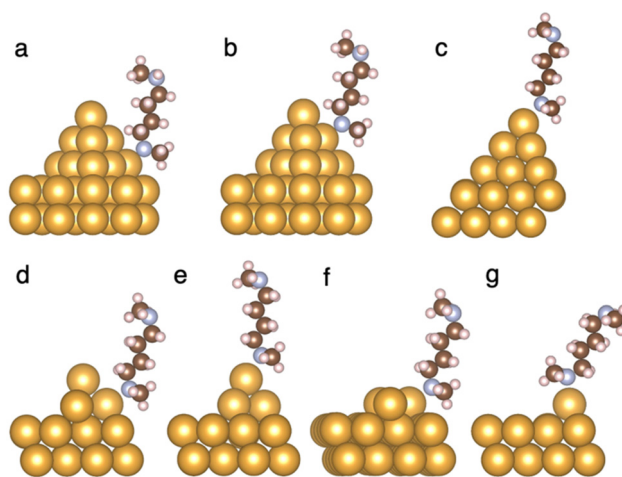
Fig. 4 (a–g) Binding configurations between **1** and Au structures as described in Table 1. All local Au structures are lying on top of a four-layer Au (111) surface (only the top two layers are shown) in the binding energy calculation. The binding configurations of **2** and Au electrodes are similar. The atomic coordinates for the structures are provided in the ESI.†

amines). This trend is consistent with previous calculations[13] that analyzed the binding energies between a primary amine and different Au surface structures.

Furthermore, comparing the different binding energies with Au for **1** and **2**, we find that **1** binds more strongly to Au than **2** when the binding site is closer to the pinnacle of the local Au structure: as Table 1 shows, **1**–Au binding is stronger than **2**–Au binding

Table 1 Binding energies in eV, between primary amine (**2**) or secondary amine (**1**) and different Au local structures, calculated using DFT

Nitrogen binds to	2	1	Fig.
Base of a three-layer Au pyramid	0.73	0.65	4(a)
Middle layer of a three-layer Au pyramid	0.62	0.65	4(b)
Top Au atom of a three-layer Au pyramid	0.59	0.61	4(c)
Base of a two-layer Au pyramid	0.76	0.72	4(d)
Top Au atom of a two-layer Au pyramid	0.64	0.68	4(e)
Au trimer	0.80	0.75	4(f)
Au adatom	0.83	0.87	4(g)

when the contact between the amine and the Au electrode is an Au adatom, the top Au atom of a two-layer Au pyramid, and the top Au atom and the middle layer of a three-layer Au pyramid. Combining this trend with the experimental observation that a wax-coated Au tip enhances binding for **1**, we conclude that the wax-coated Au tip produces more local Au surface structures that resemble an Au adatom, *via*, *e.g.*, a more exhaustive sampling of the contact geometry, as evidenced by the longer time spent in a junction (*i.e.* the longer plateau lengths), shown in Fig. S9 and S10 (ESI†). This result highlights the importance of the atomic configurations of Au in making contact with amines, and demonstrates that in certain cases, the secondary amines that carry an extra methyl group can even bind more strongly to Au than the primary amines.

We note that the conductance peak values measured in TCB and in PC are the same for **1** and **2**, around $10^{-3}G_0$. The similarity in the conductance values for **1** and **2** junctions (relaxed structures are shown in Fig. 5a, where a trimer binding motif is used; similar results are obtained for Au adatoms) is confirmed by both DFT (Fig. S11, ESI†) and DFT+Σ (Fig. 5b) calculations (see ESI† for computational details).[13,14] In DFT+Σ, we achieve a more accurate determination of the transport properties, as the energy level alignment in the junction is corrected by a self-energy Σ, following procedures as detailed previously.[15] The calculated conductance is around $4.2 \times 10^{-4}G_0$ for both junctions. Furthermore, DFT+Σ predicts that the $T(E)$ curves are almost flat around the Fermi level (Fig. 5b) for both the primary and secondary amine-linked junctions, indicating that the measured conductance values depend only weakly on the applied bias voltage, consistent with our experimental findings.

In this study, we present a novel experimental approach for enabling the use of secondary amines as chemical linker groups in single-molecule devices. By applying a wax-coated Au tip, we are able to realize robust binding between secondary amines and Au electrodes that was previously inaccessible. In detail, a more complete set of contact geometries is sampled during the measurements when a wax-coated tip is used, generating local Au surface structures similar to adatoms, resulting in an improved accessibility of N lone pairs in secondary amines to Au atoms and increased stability of the molecular junction. Our results further demonstrate that once a N–Au interaction is established, secondary amines are nearly identical to primary amines as far as transport properties are concerned, as confirmed by DFT calculations. This study highlights the intricate role that the atomic configuration of the metal plays in regulating the metal–molecule interactions and expands our toolkit in enabling new chemical groups to form robust interactions between organic materials and metal contacts.

Conflicts of interest

There are no conflicts to declare.

References

1 T. A. Su, M. Neupane, M. L. Steigerwald, L. Venkataraman and C. Nuckolls, *Nat. Rev. Mater.*, 2016, **1**(3), 16002.
2 L. Venkataraman, J. E. Klare, C. Nuckolls, M. S. Hybertsen and M. L. Steigerwald, *Nature*, 2006, **442**(7105), 904–907.
3 M. S. Hybertsen, L. Venkataraman, J. E. Klare, A. C. Whalley, M. L. Steigerwald and C. Nuckolls, *J. Phys.: Condens. Matter*, 2008, **20**(37), 374115.
4 L. Venkataraman, J. E. Klare, I. W. Tam, C. Nuckolls, M. S. Hybertsen and M. L. Steigerwald, *Nano Lett.*, 2006, **6**(3), 458–462.
5 Y. Zang, A. Pinkard, Z. F. Liu, J. B. Neaton, M. L. Steigerwald, X. Roy and L. Venkataraman, *J. Am. Chem. Soc.*, 2017, **139**(42), 14845–14848.
6 Y. S. Park, A. C. Whalley, M. Kamenetska, M. L. Steigerwald, M. S. Hybertsen, C. Nuckolls and L. Venkataraman, *J. Am. Chem. Soc.*, 2007, **129**(51), 15768–15769.
7 B. Zhang, M. H. Garner, L. Li, L. M. Campos, G. C. Solomon and L. Venkataraman, *Chem. Sci.*, 2021, **12**(30), 10299–10305.
8 B. Xu and N. J. Tao, *Science*, 2003, **301**(5637), 1221–1223.
9 B. Capozzi, J. Xia, O. Adak, E. J. Dell, Z.-F. Liu, J. C. Taylor, J. B. Neaton, L. M. Campos and L. Venkataraman, *Nat. Nanotechnol.*, 2015, **10**(6), 522–527.
10 C. Wei, J. Ye, Y. Su, J. Zheng, S. Xiao, J. Chen, S. Yuan, C. Zhang, J. Bai and H. Xu, *CCS Chemistry*, 2022, 1–9.
11 M. Huang, L. Yu, M. Zhang, Z. Wang, B. Xiao, Y. Liu, J. He and S. Chang, *Small*, 2021, **17**(36), e2101911.
12 A. I. Yanson, G. R. Bollinger, H. E. van den Brom, N. Agraït and J. M. van Ruitenbeek, *Nature*, 1998, **395**(6704), 783–785.
13 S. Y. Quek, L. Venkataraman, H. J. Choi, S. G. Louie, M. S. Hybertsen and J. Neaton, *Nano Lett.*, 2007, **7**(11), 3477–3482.
14 J. B. Neaton, M. S. Hybertsen and S. G. Louie, *Phys. Rev. Lett.*, 2006, **97**(21), 216405.
15 Z.-F. Liu, S. Wei, H. Yoon, O. Adak, I. Ponce, Y. Jiang, W.-D. Jang, L. M. Campos, L. Venkataraman and J. B. Neaton, *Nano Lett.*, 2014, **14**(9), 5365–5370.
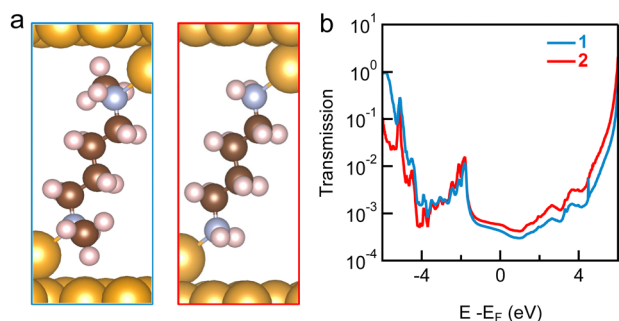
Fig. 5 (a) Relaxed structures and (b) transmission curves of **1** and **2** calculated using DFT+Σ.